Wave reflections from duct terminations

A. Selamet and Z. L. Ji
Department of Mechanical Engineering and The Center for Automotive Research, The Ohio State University, Columbus, Ohio 43210-1107

R. A. Kach
Powertrain Operations, Ford Motor Company, Dearborn, Michigan 48121

(Received 12 October 2000; accepted for publication 18 December 2000)

The reflection coefficients and inertial end corrections of several duct terminations, including finite length duct extensions perpendicular to an infinite wall, as well as at a number of angles, curved interface surfaces, and annular cavities, are determined and analyzed in the absence of flow by employing the boundary element method. Predictions for the classical unflanged and flanged circular ducts show good agreement with analytical and computational results available in the literature. The predictions for curved interface surfaces (bellmouth or horn) are also consistent with the available experimental data. In view of its high reflection coefficient, the duct termination with an annular cavity may be suggested for the suppression of noise radiation in a specific frequency band or for an effective wave reflection from the termination. © *2001 Acoustical Society of America.* [DOI: 10.1121/1.1348298]

PACS numbers: 43.20.Mv [ANN]

I. INTRODUCTION

Part of the acoustic wave reaching a duct exit is reflected back to the source and the remainder radiates into the surroundings, presenting a coupled phenomenon between the sound propagation in the duct and external sound radiation at this boundary. The reflection and radiation characteristics depend strongly on the geometry of duct termination. Thus, the reflection coefficient amplitude and the inertial end correction (or the complex reflection coefficient) of duct termination are the important parameters for the complete acoustic analysis of duct system.

For an infinite circular duct without flange, Levine and Schwinger[1] presented an elaborate analytical derivation for the reflection coefficient and end correction in the absence of mean flow. While the numerical results were given as a function of Helmholtz number, $H \equiv ka$, the limiting value of the end correction δ was determined to be $\delta/a = 0.6133$ as $H \to 0$, with k being the wave number and a the duct radius. Davies *et al.*[2] provided empirical fits to end correction of Ref. 1 as $\delta/a = 0.6133 - 0.1168H^2$ for $H < 0.5$ and $\delta/a = 0.6393 - 0.1104H$ for $0.5 < H < 2$.

For a circular duct with an infinite rigid flange, Rayleigh[3] obtained an approximate value of the end correction as $\delta/a = 0.824\,22$, while Daniell[4] provided the bounds as $0.821\,41 < \delta/a < 0.821\,68$ at zero frequency. This estimate was later recalculated by Nomura *et al.*[5] as $\delta/a = 0.8217$, by Kergomard and Garcia[6] as $\delta/a = 0.261\,53\pi = 0.821\,62$, and by Norris and Sheng[7] as $\delta/a = 0.821\,59$. Nomura *et al.*[5] used Weber–Schafheitlin integrals and Jacobi polynomials to derive a coupled system of two infinite sets of linear equations for the unknowns, which are then solved numerically. An approximate expression, $\delta/a = 0.8217 - 0.367H^2$, was provided by Peters *et al.*[8] for $H < 0.5$. Norris and Sheng[7] also presented an analytical approach for this configuration. While the method also involves numerical computation, only a single set of equations needs to be solved for the modal amplitudes in the duct. They implemented a rational function approximation to get the expressions for the reflection coefficient and end correction of the flanged and unflanged ducts. Ando[9] and Peters *et al.*[8] included the effect of duct wall thickness on the reflection coefficient and end correction. Their studies have demonstrated that, as the thickness of the duct wall is increased, these two quantities vary between the limits of the unflanged duct and infinite flanged duct at lower Helmholtz numbers. Ando's work has been reconsidered later by Bernard and Denardo.[10] Peters *et al.*[8] also experimentally investigated the reflection coefficient and end correction of a duct terminated by a horn with a radius of curvature twice the duct diameter. Their measurements revealed $\delta/a \cong 2.3$ for low H, and an increasing δ/a with increasing H for $H < 0.3$.

While the foregoing studies have provided information for some basic configurations, there remains a significant need to determine the reflection coefficient and the end correction for a number of other duct terminations that are frequently encountered in practice. The objective of the present study is then to calculate and analyze these two quantities for a chosen set of duct terminations, including finite-length duct extensions (perpendicular as well as at an oblique angle to the wall), bellmouthed interfaces, and interfaces with annular cavities.

Following the Introduction, Sec. II provides the formulation for the calculation of reflection coefficient amplitude and inertial end correction of duct termination, and Sec. III develops a numerical approach based on the subdomain boundary element method. The results from the predictions are discussed in Sec. IV. The study is concluded with final remarks in Sec. V.

II. FORMULATION

The duct terminations considered in this study include (1) a finite duct, (2) an extended duct from an infinite rigid

wall, (3) a duct with bellmouth, (4) a duct with annular uniform cavity, and (5) a duct with annular step cavity. Assuming plane wave propagation in the duct, the acoustic load impedance of duct may be expressed as

$$Z_l = \frac{p_l}{\rho c \nu_l} = \frac{Z_r \cos(kl) + j \sin(kl)}{jZ_r \sin(kl) + \cos(kl)}, \tag{1}$$

where p_l and ν_l are the acoustic pressure and velocity, ρ is the density, c is the speed of sound, Z_r is the equivalent radiation impedance at the exit, k is the wave number, l is the length of the duct, and j is the imaginary unit. Equation (1) may be rearranged to solve for Z_r as

$$Z_r = \frac{Z_l \cos(kl) - j \sin(kl)}{\cos(kl) - jZ_l \sin(kl)}. \tag{2}$$

The complex reflection coefficient R at the exit of duct can then be expressed in terms of Z_r as

$$R = -|R| \exp(-j2k\delta) = \frac{Z_r - 1}{Z_r + 1}, \tag{3}$$

where δ is the inertial end correction of the duct. Thus, once Z_l is determined, Eq. (2) gives Z_r and Eq. (3) the reflection coefficient amplitude $|R|$ and the inertial end correction δ. To evaluate the acoustic load impedance Z_l that accounts for the multidimensional waves, particularly in the neighborhood of duct exit, a subdomain boundary element approach is developed, as described next.

III. NUMERICAL APPROACH

To employ the boundary element method in determining the acoustic load impedance of the duct, the sound field is first divided into the internal and the external acoustic domains separated by the opening surface.

A. Internal acoustic domain

The internal domain may also be divided into several subdomains. For the internal domain or each subdomain, the boundary integral expression is represented[11] as

$$C(X)P(X) = \int_\Gamma \left[G(X,Y) \frac{\partial P}{\partial n}(Y) - P(Y) \frac{\partial G}{\partial n}(X,Y) \right] d\Gamma(Y), \tag{4}$$

where Γ is the boundary surface of the acoustic domain, n is the unit normal vector on Γ directed away from the domain, the function $G(X,Y) = \exp(-jkR)/4\pi R$ is Green's function of free space, R being the distance between any two points X and Y in the domain or on the surface, and $C(X)$ is a coefficient which depends on the position of point X and may be evaluated[11] by

$$C(X) = \int_\Gamma \frac{\partial}{\partial n} \left(\frac{1}{4\pi R} \right) d\Gamma(Y). \tag{5}$$

A numerical solution of the boundary integral Eq. (4) can be achieved by discretizing the boundary surface of the domain into a number of elements. By using discretization and numerical integration, the following algebraic system of equations is obtained[11]

$$[F]\{P\} = \rho c [G]\{V\}, \tag{6}$$

where $[F]$ and $[G]$ are the coefficient matrices, and $\{P\}$ and $\{V\}$ are the vectors of sound pressure and outward normal particle velocity at boundary nodes, respectively, ρc is the characteristic impedance of the medium. The boundaries are grouped into the inlet, opening and wall, represented by the subscripts i, o, and w, respectively. Equation (6) combined with the rigid wall boundary condition yields[12]

$$\begin{Bmatrix} P_i^d \\ P_o^d \end{Bmatrix} = \rho c [T^d] \begin{Bmatrix} V_i^d \\ V_o^d \end{Bmatrix}, \quad \text{(for the duct)}, \tag{7}$$

$$\{P_o^c\} = \rho c [T^c]\{V_o^c\}, \quad \text{(for the cavity)}. \tag{8}$$

Combining duct and cavity gives

$$\begin{Bmatrix} P_i^d \\ P_o^i \end{Bmatrix} = \rho c [T^i] \begin{Bmatrix} V_i^d \\ V_o^i \end{Bmatrix}, \tag{9}$$

where

$$\{P_o^i\} = \begin{Bmatrix} P_o^d \\ P_o^c \end{Bmatrix}, \quad \{V_o^i\} = \begin{Bmatrix} V_o^d \\ V_o^c \end{Bmatrix},$$

and

$$[T^i] = \begin{bmatrix} T^d & 0 \\ 0 & T^c \end{bmatrix}$$

is the transfer impedance matrix between the inlet and opening for the internal acoustic domain.

B. External acoustic domain

For the full-space external sound field, the boundary integral expression is represented[11] as

$$C^e(X)P^e(X) = \int_\Gamma \left[G(X,Y) \frac{\partial P^e}{\partial n}(Y) - P^e(Y) \frac{\partial G}{\partial n}(X,Y) \right] d\Gamma(Y), \tag{10}$$

$$C^e(X) = 1 - \int_\Gamma \frac{\partial}{\partial n} \left(\frac{1}{4\pi R} \right) d\Gamma(Y). \tag{11}$$

Similar to the formulation of internal acoustics, discretization and numerical integration of Eq. (10) lead to the following algebraic system of equations:

$$[F^e]\{P^e\} = \rho c [G^e]\{V^e\}. \tag{12}$$

The boundaries are grouped into the opening and wall, represented by subscripts o and w, respectively. Equation (12) combined with the rigid wall boundary condition yields

$$\{P_o^e\} = \rho c [T^e]\{V_o^e\}, \tag{13}$$

$[T^e]$ being the radiation impedance matrix for the external acoustic domain.

For the external acoustic domain with duct extension from an infinite rigid wall, the boundary integral equation can be written[11] as

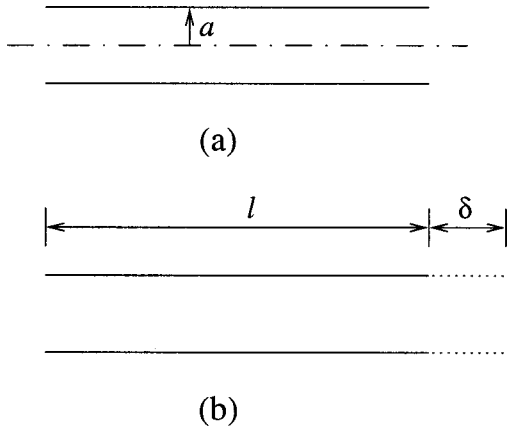

FIG. 1. Unflanged finite duct.

$$C^e(X)P^e(X)=\int_{\Gamma_w+\Gamma_o}\left[G_H(X,Y)\frac{\partial P^e}{\partial n}(Y)-P^e(Y)\frac{\partial G_H}{\partial n}(X,Y)\right]d\Gamma(Y), \tag{14}$$

where Γ_w is the wall of extended duct from the infinite wall, Γ_o is the opening,

$$G_H=\frac{\exp(-jkR)}{4\pi R}+\frac{\exp(-jkR_1)}{4\pi R_1}$$

is the half-space Green's function, R_1 being the distance between Y and the image point of X with respect to the flange; and

$$C^e(X)=1-\int_\Gamma\frac{\partial}{\partial n}\left(\frac{1}{4\pi R}\right)d\Gamma(Y), \tag{15}$$

Γ being the total boundary of the duct extended from the infinite wall. Similar to the full-space problem, the acoustic radiation impedance matrix $[T^e]$ for this case can be obtained by using discretization and numerical integration of Eq. (14). For the limiting case of no-extension (a duct with infinite rigid flange), the sound pressure at the opening may be expressed as

$$P^e(X)=\int_{\Gamma_o}\left[\frac{\exp(-jkR)}{2\pi R}\frac{\partial P^e}{\partial n}(Y)\right]d\Gamma(Y). \tag{16}$$

Similarly, the acoustic radiation impedance matrix $[T^e]$ for the semi-infinite external acoustic domain can also be obtained by using discretization and numerical integration of Eq. (16).

C. Coupling

At the opening, the solution should satisfy the continuity conditions of sound pressure and particle velocity:

$$\{P_o^e\}=\{P_o^i\}, \tag{17}$$

$$\{V_o^e\}=-\{V_o^i\}. \tag{18}$$

Combining Eqs. (9) and (13) with the continuity conditions (17) and (18) yields the acoustic load impedance as

$$Z_l=[T_{11}^i-T_{12}^i(T_{22}^i+T^e)^{-1}T_{21}^i]. \tag{19}$$

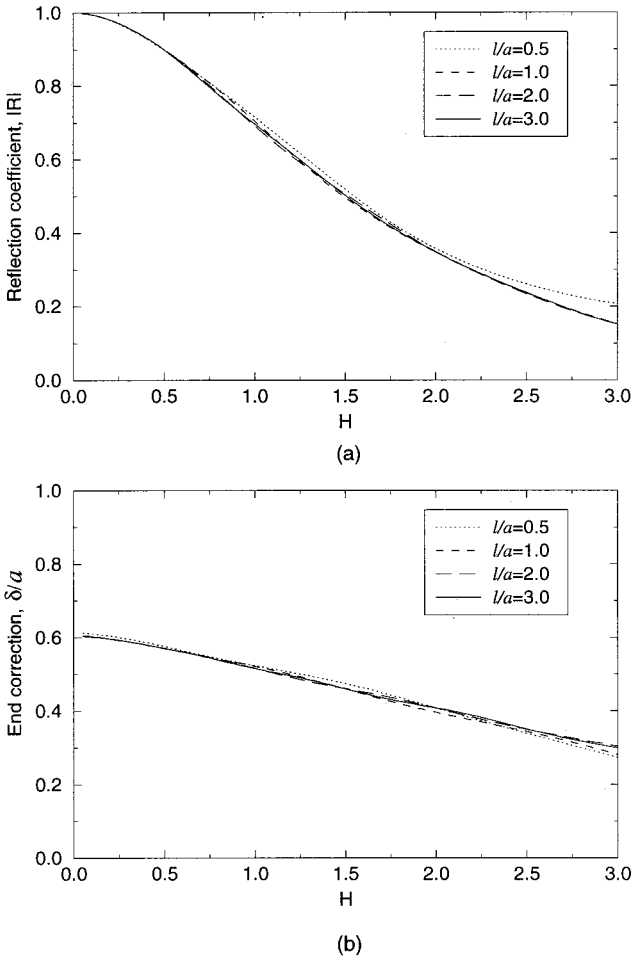

FIG. 2. Unflanged finite duct: (a) reflection coefficient and (b) end correction.

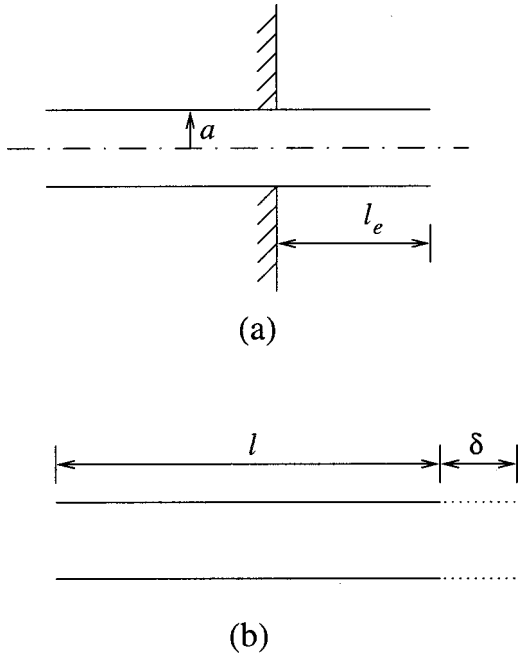

FIG. 3. Duct extended from an infinite rigid flange.

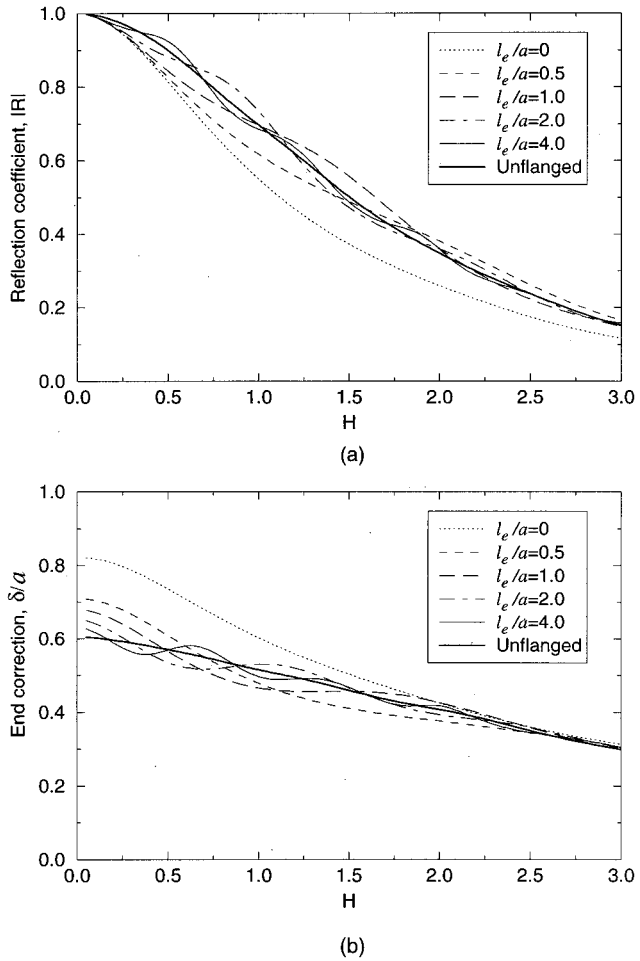

FIG. 4. Duct extended from an infinite rigid flange: (a) reflection coefficient and (b) end correction.

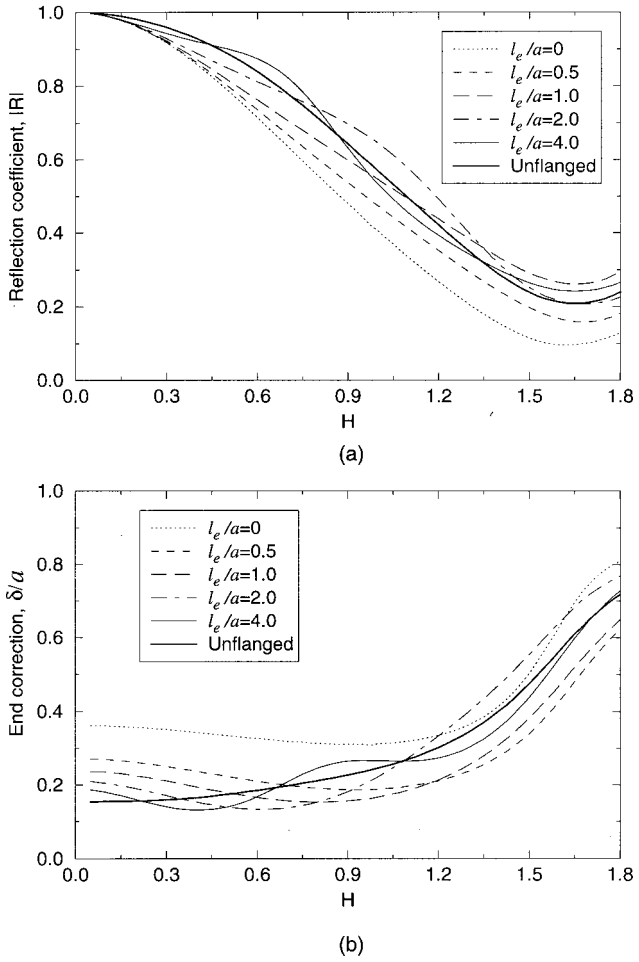

FIG. 6. Duct at an angle $\theta=45°$ extended from an infinite rigid flange: (a) reflection coefficient and (b) end correction.

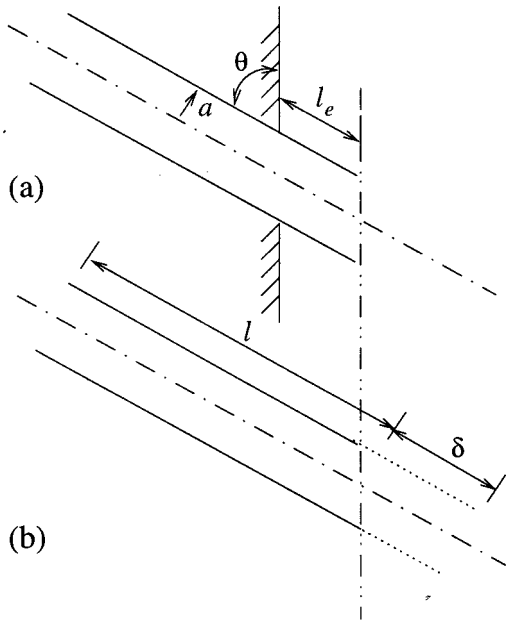

FIG. 5. Duct at an angle θ extended from an infinite rigid flange.

IV. RESULTS AND DISCUSSION

First, the effect of length of an unflanged finite duct (Fig. 1) on the reflection coefficient and end correction is examined. Figure 2 shows the numerical predictions of reflection coefficient and end correction for four different duct lengths ($l/a=0.5, 1.0, 2.0, 3.0$). For a duct with $l/a>2$, the results illustrate that the effect of duct length on these two quantities becomes negligible in the region of $H<3$, and the present predictions agree with the analytical results of Levine and Schwinger[1] for the classical configuration of the infinite duct without flange.

The effect of duct extension l_e from the infinite rigid wall (Fig. 3) on the reflection coefficient and end correction is shown in Fig. 4. The finite extension introduces an oscillatory behavior on both quantities as a function of H due to the presence of an infinite rigid wall. The period of oscillations in H may be crudely (via a one-dimensional argument) related to two subsequent quarter wave resonances between the duct opening and the infinite rigid wall leading to $\Delta H \cong \pi/[(l_e+\delta)/a]$. As expected, the oscillatory behavior diminishes as l_e/a becomes large. For the limiting case of no-extension ($l_e/a=0$, flanged duct), the present predictions of the reflection coefficient and end correction are in good agreement with the available literature (Rayleigh,[3] Daniell,[4]

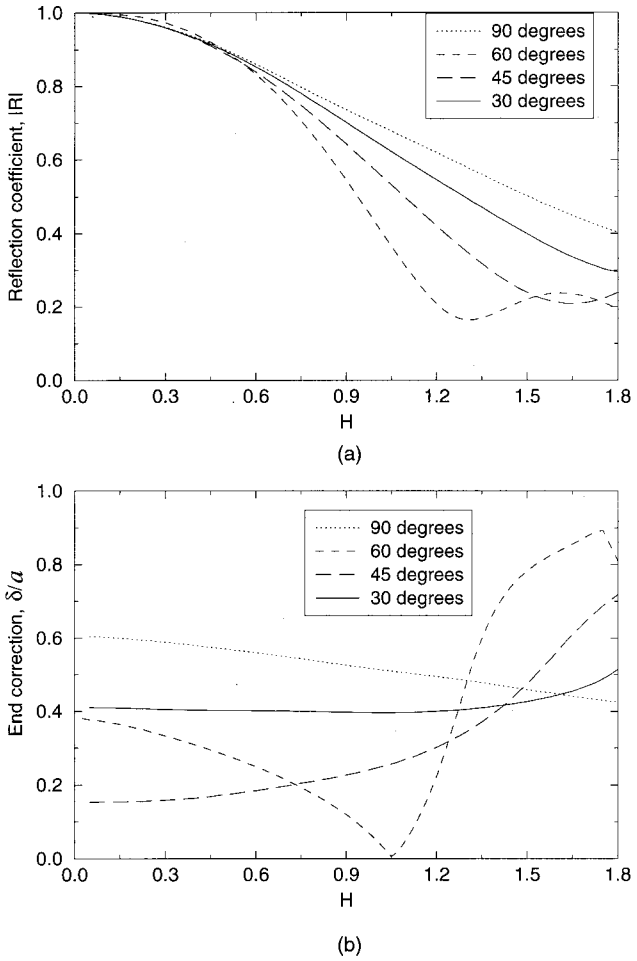

FIG. 7. Unflanged ducts with θ=30°,45°,60°,90°: Comparison of (a) reflection coefficient and (b) end correction.

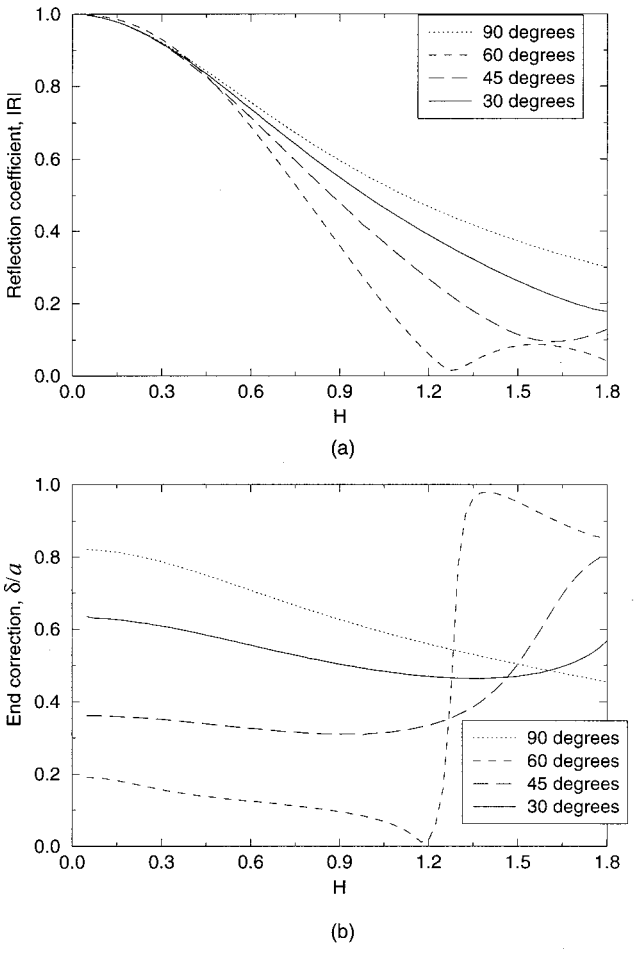

FIG. 8. Flanged ducts with $l_e=0$ and θ=30°,45°,60°,90°: Comparison of (a) reflection coefficient and (b) end correction.

Nomura *et al.*,[5] Kergomard and Garcia,[6] and Norris and Sheng[7]). The present predictions in Fig. 4(b) for $l_e/a=0$ agree very well with Fig. 7 of Nomura *et al.*[5] to the degree that the two sets of results cannot be distinguished from each other over $0<H<3.0$, including, for example, a specific value of $\delta/a=0.821$ for $H=0.05$.

The predictions for the reflection coefficient and end correction for a duct extension from an infinite rigid wall with an oblique angle of θ (Fig. 5) are shown in Fig. 6 for θ=45°. Similar to the duct extension with 90° angle, the oscillatory behavior is observed again. Figures 7 and 8 compare the reflection coefficients and end corrections for, respectively, the unflanged and flanged ducts with $l_e=0$ and θ=30°,45°,60°,90°. At higher Helmholtz numbers ducts with larger θ provide, in general, higher reflection coefficients. In view of the definition of δ in Fig. 5, a reduction on the order of radius may be anticipated for θ=45° (relative to θ=90°) at low Helmholtz numbers as shown in Fig. 7. Note that $H \leqslant 1.8$ in Figs. 6–8 to remain below the first diametral mode (1,0).

The acoustic characteristics of a duct with bellmouth (Fig. 9) are examined next to understand the effect of radius of curvature on the reflection coefficient and end correction. The latter is defined relative to the end of the straight section of the duct, consistent with Peters *et al.*[8] Figures 10 and 11 depict the computed results for these two quantities for five different radii of curvature (r/a=0.5,1.0,2.0,3.0,4.0), and without and with an infinite flange, respectively. With increasing radius of curvature, the reflection coefficient decreases and the end correction increases. For the special case of $r/a=4$, the present predictions agree with the experimental results of Peters *et al.*[8] who determined $\delta/a \cong 2.3$ at low values of H. For this special case at $H=0.025$, for example, the predicted numerical values are $\delta/a=2.322$ and

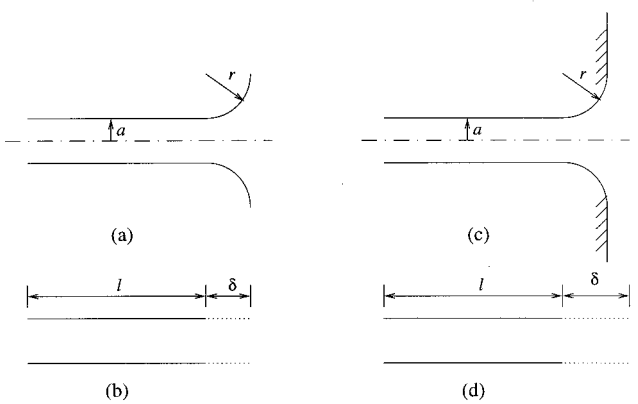

FIG. 9. Ducts with unflanged and flanged bellmouth.

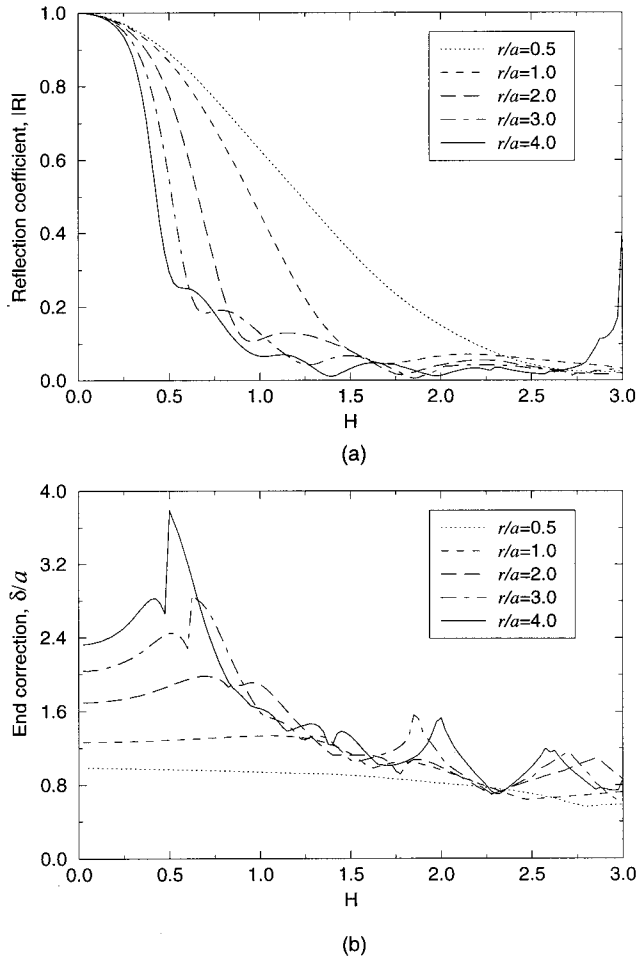

FIG. 10. Duct with unflanged bellmouth: (a) reflection coefficient and (b) end correction.

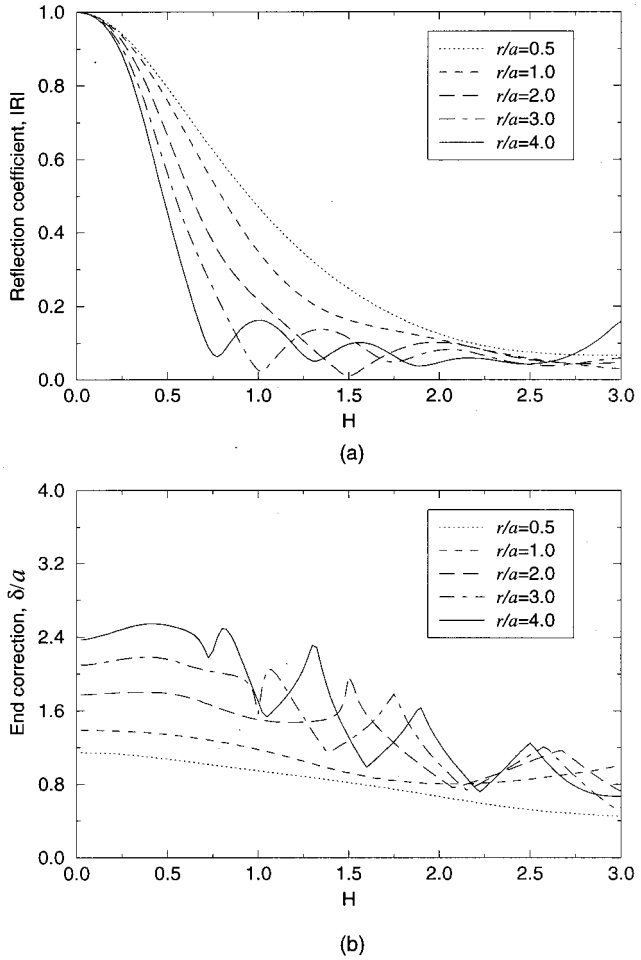

FIG. 11. Duct with flanged bellmouth: (a) reflection coefficient and (b) end correction.

$\delta/a=2.369$ for Fig. 10(b) and Fig. 11(b), respectively. The differences in these configurations beyond the radiused inlet do not have a significant impact on the end correction for low H. In comparison with the straight duct, the duct with bellmouth leads to much lower wave reflection at higher Helmholtz numbers. Thus the bellmouth with large radius of curvature should be avoided, for example, at the exhaust exit in order to promote effective pressure reflections from the termination for noise control. Figure 12 shows the effect of curved interface with the radiused length subtracted from the end correction, transforming the dimensionless end correction to $(\delta-r)/a$. Such manipulation essentially shifts the reference point for end correction to the very end of the duct (end of bellmouth section). Relative to the end of the curved duct, Fig. 12 then suggests that a duct with a large-radius termination, such as $r/a=4$, will appear to be shorter than the actual total length when the end correction is incorporated.

Finally, ducts with annular cavities (unflanged and flanged) are considered as shown in Fig. 13 with a constant cross section and Fig. 14 with a step transition. The computed results for the reflection coefficient and the end correction are compared in Fig. 15 for $l_c/c=4$ and $c/a=1/2$. The results with cavities here may be contrasted with the ducts alone of Figs. 2 and 4. As a result of the interaction of waves reflected from attached cavities with those radiated from the opening, it is important to note that (1) the behavior of reflection coefficient changes dramatically including the additional peaks, therefore the sound radiation may be suppressed effectively in a specific frequency band, and/or (2) the pressure wave reflections from the termination back to the duct would be strengthened. Compared to the uniform cavity, the step cavity moves the first additional peak to a higher Helmholtz number, and the second peak to a lower Helmholtz number. The high reflection coefficient, in a specific frequency band, of duct with annular cavity may be used to compensate the low attenuation in the corresponding frequency region of a silencer, therefore an improved acoustic attenuation performance may be obtained. Similar behavior can possibly be utilized to promote stronger pressure wave reflections from the opening, thereby providing mechanisms to manipulate engine tuning.

V. CONCLUDING REMARKS

This study has shown the effect of duct termination geometry on the reflection coefficient and the inertial end correction by employing the subdomain boundary element approach. These two quantities were determined and analyzed for (1) an unflanged finite duct, (2) a duct extended from an infinite rigid wall, (3) a duct extended with an angle θ from

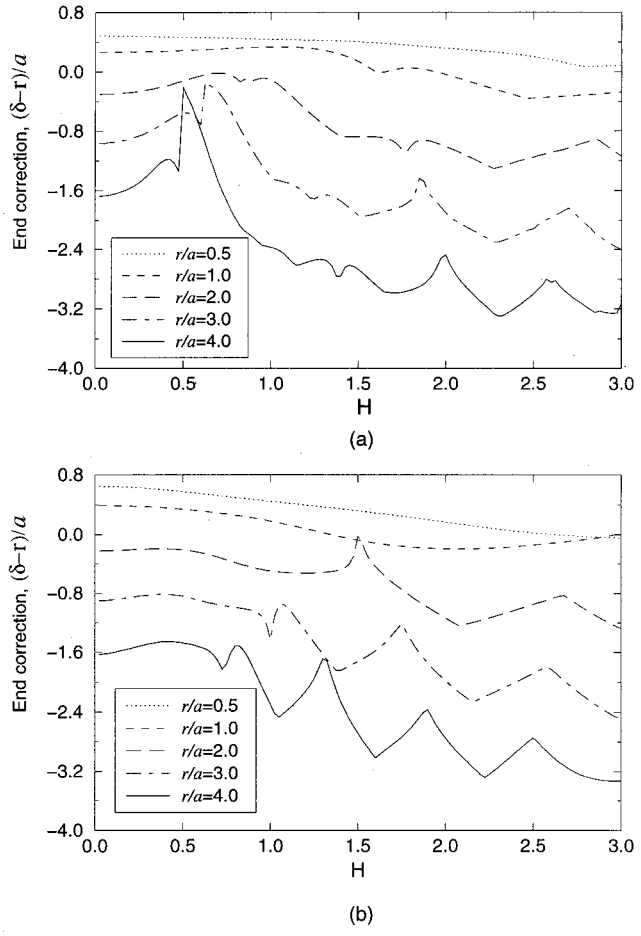

FIG. 12. $(\delta - r)/a$ for ducts with (a) unflanged bellmouth and (b) flanged bellmouth.

an infinite rigid wall, (4) ducts with unflanged and flanged bellmouth, and (5) ducts with unflanged and flanged annular cavities. The effect of flow, which was well established in the literature for certain configurations (see, for example, Peters *et al.*[8]), as a function of Mach and Strouhal numbers was excluded from the study. Instead, the current work has chosen to concentrate on quantifying the impact of interface geometry which has not been investigated in detail with the exception of limiting cases. For unflanged configurations, a finite duct with $l/a > 2$ exhibits similar acoustic characteris-

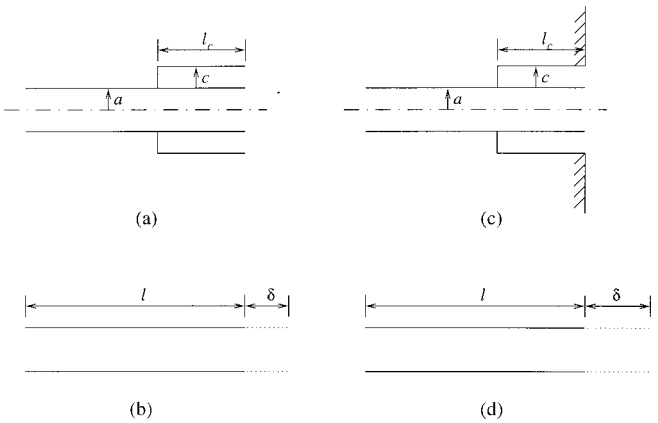

FIG. 13. Ducts with unflanged and flanged annular uniform cavity.

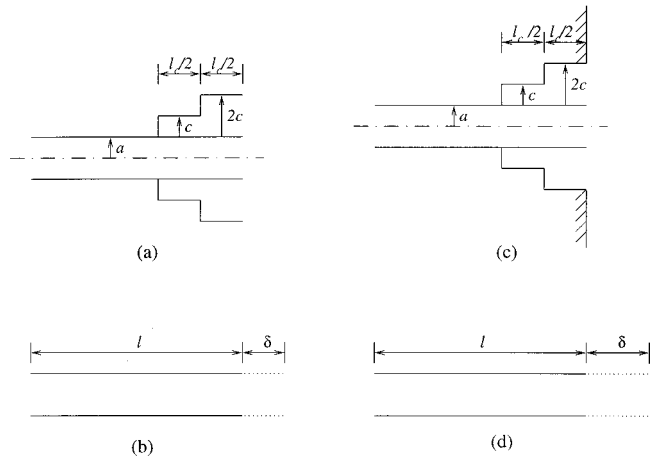

FIG. 14. Ducts with unflanged and flanged annular step cavity.

tics to an infinite duct at low Helmholtz numbers. The duct extension from an infinite rigid wall introduces an oscillatory behavior in the reflection coefficient and end correction near the baseline unflanged duct due to the interaction of waves reflected from the infinite wall and those radiated from the duct opening. Within about a diameter-distance from the

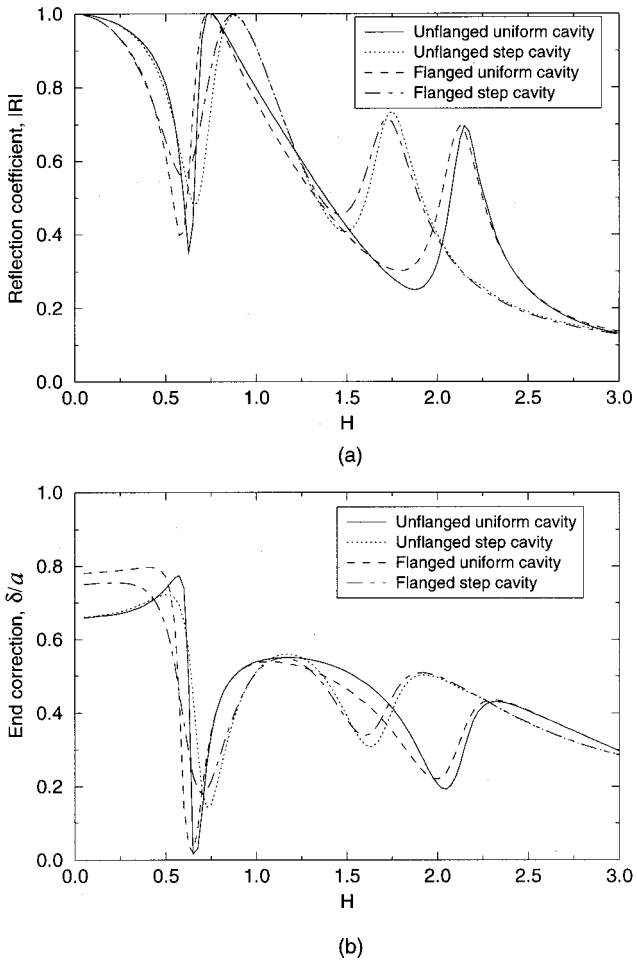

FIG. 15. Ducts with unflanged and flanged annular cavity with $l_c/c = 4$ and $c/a = 1/2$: (a) reflection coefficient and (b) end correction.

wall, the acoustic behavior of the two quantities approaches that of an unflanged wall with the exception of oscillations. The oblique duct extension from an infinite rigid wall, in general, decreases the reflection coefficient of a duct at higher Helmholtz numbers as compared to the perpendicular extension. The bellmouth interface reduces the reflection coefficient significantly at higher Helmholtz numbers. The duct termination with cavity influences end correction and introduces additional peaks in the reflection coefficient and may be used for the suppression of noise radiation, or to promote effective wave reflection from the open end.

[1] H. Levine and J. Schwinger, ''On the radiation of sound from an unflanged circular pipe,'' Phys. Rev. **73**, 383–406 (1948).

[2] P. O. A. L. Davies, J. L. Bento Coelho, and M. Bhattacharya, ''Reflection coefficients for an unflanged pipe with flow,'' J. Sound Vib. **72**, 543–546 (1980).

[3] Lord Rayleigh, *The Theory of Sound* (Dover, New York, 1945).

[4] P. J. Daniell, ''The coefficient of end-correction,'' Philos. Mag. **30**, 137–146, 248–256 (1915).

[5] Y. Nomura, I. Yamamura, and S. Inawashiro, ''On the acoustic radiation from a flanged circular pipe,'' J. Phys. Soc. Jpn. **15**, 510–517 (1960).

[6] J. Kergomard and A. Garcia, ''Simple discontinuities in acoustic waveguides at low frequencies: Critical analysis and formulae,'' J. Sound Vib. **114**, 465–479 (1987).

[7] A. N. Norris and I. Sheng, ''Acoustic radiation from a circular pipe with an infinite flange,'' J. Sound Vib. **135**, 85–93 (1989).

[8] M. C. A. M. Peters, A. Hirschberg, and A. J. Reijnen, ''Damping and reflection coefficient measurements for an open pipe at low Mach and low Helmholtz numbers,'' J. Fluid Mech. **256**, 499–534 (1993).

[9] Y. Ando, ''On the acoustic radiation from semi-infinite circular pipe of certain wall thickness,'' Acustica **22**, 219–225 (1969/1970).

[10] M. Bernard and B. Denardo, ''Re-computation of Ando's approximation of the end correction for a radiating semi-infinite circular pipe,'' Acustica **82**, 670–671 (1996).

[11] R. D. Ciskowski and C. A. Brebbia, *Boundary Element Methods in Acoustics* (Computational Mechanics Publications, Boston, 1991).

[12] Z. L. Ji, Q. Ma, and Z. H. Zhang, ''Application of the boundary element method to predicting acoustic performance of expansion chamber mufflers with mean flow,'' J. Sound Vib. **173**, 57–71 (1994).